UPDATES TO THE NEQAIR RADIATION SOLVER

Brett A. Cruden[(1)], Aaron M. Brandis[(1)]

[(1)]ERC Inc at NASA Ames, NASA Ames Research Center, MS 230-2, Moffett Field, CA 94035,
E-mail: Brett.A.Cruden@nasa.gov, Aaron.M.Brandis@nasa.gov

ABSTRACT

The NEQAIR code is one of the original heritage solvers for radiative heating prediction in aerothermal environments, and is still used today for mission design purposes. This paper discusses the implementation of the first major revision to the NEQAIR code in the last five years, NEQAIR v14.0. The most notable features of NEQAIR v14.0 are the parallelization of the radiation computation, reducing runtimes by about 30×, and the inclusion of mid-wave CO_2 infrared radiation.

1. INTRODUCTION

The NEQAIR code was first produced in 1985[1] by Chul Park based on the HF730 code dating from the 1970s. Since then there have been approximately 22 release versions, with major revisions appearing in 1996, 1999, 2009 and 2014. Only the 1996 version included significant documentation.[2] The intent of this paper is to provide detailed documentation regarding the implementation of specific updates found in the latest version.

The paper is arranged into six sections, each detailing a major improvement of NEQAIR v14.0. These sections include discussions of bound-free radiation, parallelization, non-local radiation modelling, tangent slab evaluation, CO_2 radiation, and issues related to inconsistencies in the treatment of the computational fluid dynamics (CFD) flowfield with the quasi-steady state (QSS) evaluation. Another change implemented in v14.0 that is not discussed here is the ability to obtain radiance perpendicular to the line of sight (i.e., shock tube mode).

2. BOUND-FREE RADIATION

Heritage versions of NEQAIR had calculated bound-free radiation by taking the Gaunt factors of Peach[3] as corrections to the hydrogenic approximation in calculating the photo-absorption coefficient. This was then converted to the bound-free emissivity using Saha equilibrium and a fictional state correction. An update in v13.2 of NEQAIR sought to replace this with the newer cross-section data of TOPBase[4] and also to correct the absorption/emission relationship to follow the principle of detailed balance. The TOPBase database consists of cross-sections for photo-absorption indexed by the absorbing level. The absorption coefficient (including stimulated emission) is calculated from this as:

$$\alpha_i^{bf} = k_{ab,i} n_i - k_{st,i} n_+ n_e \tag{1}$$

and the emission coefficient is:

$$\varepsilon_i^{bf} = k_{em,i} n_+ n_e \tag{2}$$

Detailed balance requires the following relationships to hold:

$$\begin{aligned} k_{ab,i} &= \sigma_{ab,i} \\ k_{st,i} &= \frac{g^i}{g^+} \frac{\Lambda^3}{2} \exp\left[\frac{E_+ - E_i - hc/\lambda}{kT} \right] k_{ab,i} \\ k_{em,i} &= \frac{hc^2}{\lambda^5} k_{st,i} \end{aligned} \tag{3}$$

These can be shown to obey Kirchoff's law at Saha equilibrium.

Two difficulties arose when implementing TOPBase in the heritage version of NEQAIR. First, the levels within TOPBase did not have a one to one matching with the levels tracked within NEQAIR. This is not an issue for Boltzmann distributed populations as degeneracies and energy levels in TOPBase could be used to calculate a state density. However, for quasi-steady state (QSS) solutions, it was necessary to assign each TOPBase level to a QSS state.

To handle this, code was implemented that would read a TOPBase level file and cross-check it against both the QSS level groupings and the NIST level list used by NEQAIR. To facilitate this process, code was also implemented to match the NIST and QSS level lists against each other. Previously, the equivalence between NIST and QSS lists was specified within the database files, and was essentially a manual process.

The three lists represent differing granularities for tracking atomic levels. The NIST-based level and line lists delineate the fine structure of the atomic levels. The TOPBase list groups fine structure, but separates spin and angular momentum. The QSS levels are grouped coarsely and may combine spin, angular momentum and/or principal quantum number. None of the level lists is assumed to be comprehensive, so there may exist levels that do not appear in all three groups.

In NEQAIR, the NIST and QSS levels are labeled by the configuration of the highest energy electron in the state and the equivalent L-S coupling term. The configuration contains two or three characters and is given as:

$$nL^N$$

where n is the primary quantum number, L is the orbital type (S, P, D, F, G, etc.) and N is (optionally) the occupancy. The term is limited to two characters and specifies the overall angular momentum of the state in terms of LS coupling. This term is expressed as:

$$^{g_S}L$$

where g_S is the spin degeneracy (g_s = 2S+1) and L is the orbital angular momentum quantum number (S, P, D, F, etc.). In cases where L-S coupling does not apply, NEQAIR will expect the closest applicable L-S notation. The QSS levels are grouped by specifying configuration/term pairs consecutively. The lumped level may be specified to contain all the terms within a particular configuration or all terms and configurations with a single primary quantum number.

The TOPBase levels are each indexed by 4 values, including the spin degeneracy (g_S) and orbital quantum number (L=0, 1, 2, 3...), which may be equated to the term value. The level files contain additional information which may be used to construct the configuration of each state.

The configuration and term notations separate most states, but are not completely unique. Therefore the lists are compared and matched in order of increasing energy. As levels are matched, the degeneracies of the lumped states are tracked to determine when all the individual levels and fine structure is accounted for. The QSS and TOPBase lists are first compared independently against the level list in this manner. In this process, most TOPBase levels may also be assigned a corresponding QSS state. Any levels remaining are then matched directly between TOPBase and QSS lists. Since the NIST list is more exact, the (degeneracy-weighted) average energy of the QSS and TOPBase levels are recalculated when the process is complete.

The second difficulty has to do with the number of points comprising the TOPBase cross-sections. Among atoms of interest such as C, N and O, there are up to several hundred levels per atom and hundreds to thousands of points per level. It was decided to use the TOPBase dataset as provided and not to otherwise smooth or flatten the curves. This significantly increased the calculation time over previous versions of NEQAIR which used only 10 points and on the order of 30 levels per atoms. This resulted in a run-time increase of approximately 4x in v13.2. About half of this efficiency was re-gained in v14.0 by separating terms in Eq. (3) which could be evaluated outside of the level loop. Further improvement was realized through parallelization of the code, which is discussed in the next section.

Two examples of bound-free radiation are shown in Fig. 1, one for an air re-entry condition (only N bound-free shown) and the second for a Venus entry (C bound-free only). The most obvious impact of the new databases is the increase of continuum radiance in the ultraviolet and vacuum ultraviolet due to the extension of recombination cross-section to higher energies (previous versions truncated at ~6 eV above dissociation energy), and inclusion of additional states. This ultraviolet/vacuum ultraviolet radiance for air is corroborated by shock tube measurements where the continuum in this region has been historically underpredicted.[5, 6] For the Venus case, the small

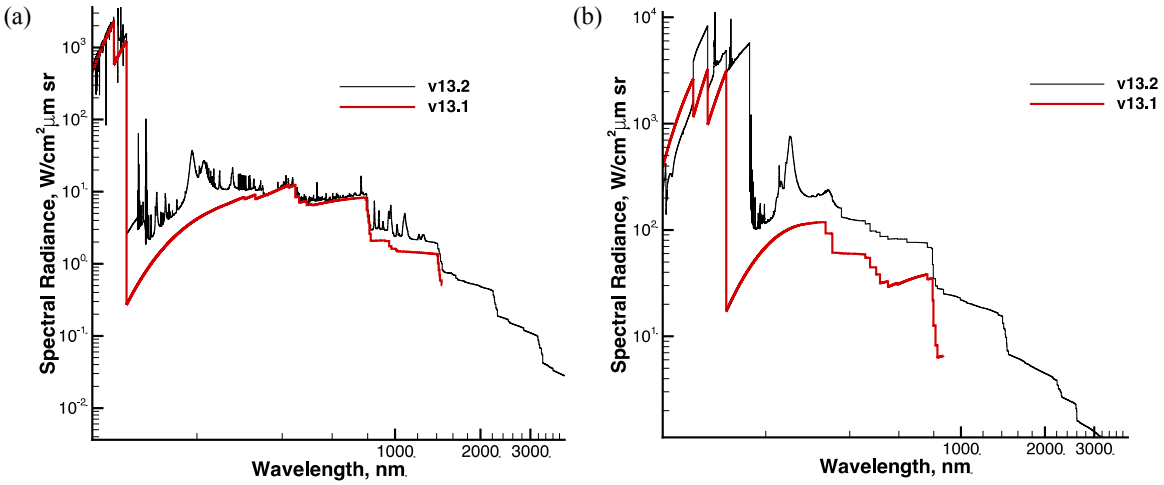

Fig. 1. Updated bound-free radiation for (a) Air entry and (b) Venus entry.

amount of existing shock tube data[7] suggests the bound-free prediction to be improved in the ultraviolet but overpredicted in the vacuum ultraviolet. Further validation work, including new shock tube data, is desired to improve this prediction.

3. PARALLELIZATION

The general schematic for solving radiation in serial and parallel is shown in Fig. 2. After reading inputs, emission and absorption coefficients are calculated at each line of sight point. In NEQAIR, this takes approximately 60% of the computation time. Next, the coefficients are integrated over an off-normal angle (i loop in Fig. 2) and line of sight point (n loop in Fig. Fig. 2) to obtain the radiation solution. The parallelization approach recognizes first that the coefficient calculations (e_λ, a_λ) are independent at each line of sight point and can be easily parallelized. Second, the radiative transport calculation is seen to consist of an exponentiation, a division, a multiplication, and two addition/subtractions. This calculation is performed for each wavelength (L), at each line of sight point (N) and for each angle required for the tangent slab evaluation (I), so the number of evaluations is (L×N×I). Two of the most time-consuming calculations do not need to be calculated in series, and thus can be parallelized, reducing the divisions and exponentiations to L and L×I calculations per processor, respectively. The less expensive addition/multiplication computations still occur sequentially.

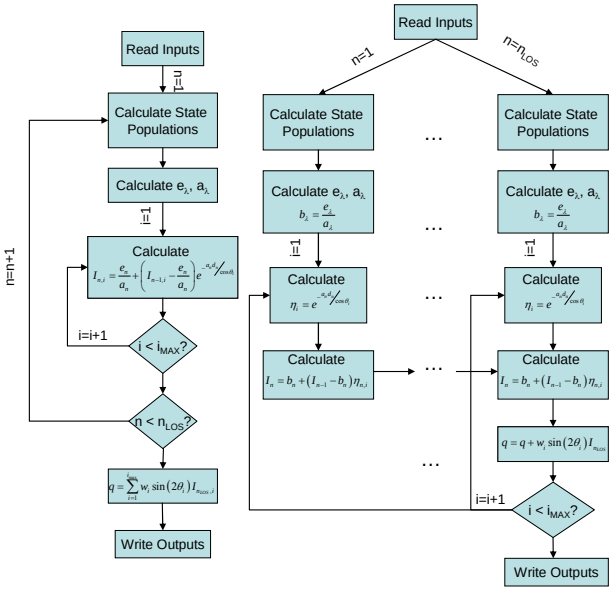

Fig. 2. Flowchart description of serial (left) and parallel (right) radiation computation, as implemented in NEQAIR.

Table I. Run times for different NEQAIR versions and test cases (in minutes), processors used (for v14.0) and improvement factor

Version	CEV	FIREII	Mars	Titan	Venus
13.1	40	18	53	22.5	23.5
13.2	140	89	212	22	74
14.0 (serial)	61	42	104	25	56
14.0	4.5	2.5	6	2	3
Improvement Factor (x)	31	36	35	11	25

The time savings from this procedure are shown in Table I for 5 of NEQAIR's standard test cases for recent versions of NEQAIR (since 2013).

4. NON-LOCAL TRANSPORT

Non-local transport refers to the fact that certain excitation/de-excitation processes are driven by the interaction of the local gas composition with the radiation field which is produced and accumulated from elsewhere in the flowfield (hence, non-local). This originates from solving the QSS equation:

$$\mathbf{Mn} = \mathbf{b}$$

$$\mathbf{M}_{ij} = \begin{cases} B_{ji}E + k^{el}_{j\to i} n_e & j < i \\ -k^{ph}_{i\to +} E - k^{el}_{i\to +} n_e - \sum_{k=1}^{i-1}\left(A_{ik} + k^{el}_{k\leftarrow i} n_e\right) - \sum_{k=i+1}^{n}\left(B_{ik}E + k^{el}_{i\to k} n_e\right) & j = i \\ A_{ji} + k^{el}_{i\leftarrow j} n_e & j > i \end{cases} \quad (4)$$

$$\mathbf{b}_i = -k^{e}_{+\to i} n_e^2 - k^{ph}_{+\to i} n_+ n_e$$

where the E in equation (4) represents the spectral radiance incident on the volume element from all directions. Determining the value of E first requires solving the QSS equation at all flowfield points, then solving the radiative transport equation from those points to the point under consideration. This radiance needs to be averaged over all possible lines of sight:

$$E = \frac{1}{4\pi}\int_0^{\pi}\int_0^{2\pi} E_{\theta\varphi} \sin\theta d\theta d\varphi \quad (5)$$

Therefore, solving non-local transport requires iteration over all points in the flowfield and is typically avoided due to computational complexity. The usual approximation employed is to introduce an escape factor which is either specified or estimated by assuming the radiance to be approximated by the local radiation coefficients accumulated over some distance *d*. This works well in many cases, but is demonstrably bad in boundary layers, the non-equilibrium shock zone and expanding flows.[8] In many cases, the error attributable to this will be diminished over a line of sight, but not for backshell heating, strongly absorbing boundary layers or very thin shock stand-offs.

Therefore, a non-local solver was introduced into NEQAIR 14.0.

Presently the non-local solver operates for atomic QSS only. The mechanics of setting up the non-local radiation field for molecular QSS are identical, however evaluation of the excitation/de-excitation requires the calculation of absorption/emission rates over entire bands rather than individual lines. This more involved calculation is planned for a future release.

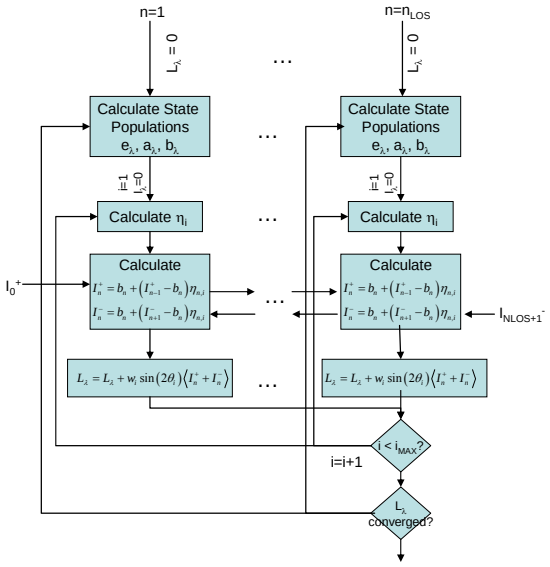

Fig. 3. Flowchart detailing the scheme for non-local solutions

The methodology for the non-local solution is shown schematically in Fig. 3. The calculation essentially places a convergence loop over the entire calculation of Fig. 2, with a few modifications. The state population calculation now uses an incident spectral irradiance, here called L_λ, which is calculated at each line of sight point. The radiance on the point (E_λ or I_λ) is given by the irradiance over 4π. On the first iteration, this value is set to zero. The evaluation of L_λ requires the radiation to be evaluated from all directions. For the 1D nature of NEQAIR, this means the solution is evaluated and passed in both directions along the line of sight, and the tangent slab approximation is employed in both directions. This requires the definition of boundary conditions at both ends of the LOS, shown as I_0^+ and I_{NLOS+1}^- in Fig. 2. There are three options for I_0^+: it may be set to zero (most common), a blackbody at temperature T_0, or an arbitrary spectral radiance. I_{NLOS+1}^- is treated as a surface at T_{NLOS}. In this case the surface emissivity and reflectivity must be specified as either constant (grey-body) or wavelength dependent values. The emissivity is used to calculate the thermal emission from the surface while the reflectivity determines the backward scattering of incident radiation I_{NLOS}^+. If emissivity and reflectivity do not sum to 1, this means some of the incident radiation will be transmitted through the surface, though this does not affect NEQAIR's calculation.

As the irradiance may change significantly throughout a single slab, a mean interior irradiance is used rather than the irradiance entering or exiting the slab. The interior irradiance is calculated so as to provide the correct excitation over the entire slab, i.e:

$$r_n^+ = \alpha_n \left\langle I^+ \right\rangle = \frac{\alpha_n}{d_n} \int_0^{d_n} I^+ dx \tag{6}$$

For a constant slab, it can be shown that:

$$\left\langle I_n^+ \right\rangle = \frac{1}{d_n} \int_0^{d_n} I^+ dx = b_n + \frac{I_{n-1}^+ - I_n^+}{\alpha_n d_n} \tag{7}$$

with a similar relation in the opposite direction.

Whether or not a non-local solution is required can be checked by running NEQAIR with the escape factor set to 0 and then again with it set to 1, as these will typically bracket the non-local answer. Example solutions obtained with escape factors of 0, 1 and local/non-local approximations for a backshell heating problem are shown in Fig. 4. Also shown are solutions where the populations are set to Boltzmann or Saha distributions. Figure 4(b) shows the state populations at one point in the simulation. The Saha distribution predicts a significantly larger excited state population because the ion and electron densities are well in excess of equilibrium in backshell cases. This large excited state population leads to significantly larger heating magnitude, particularly due to the resonant VUV lines. The Boltzmann distribution, on the other hand, puts excited states in equilibrium with the ground state, so it results in much lower radiance.

The QSS prediction calculates the balance of interactions involving the ground and ionized states, so it yields distributions between these two values. Ionization processes will favor the Saha distribution, while bound-bound radiation and collisional excitations involving the ground state will tend toward the Boltzmann distribution. When the escape factor is unity, radiative transitions are maximized, causing the distribution to be closer to Boltzmann than the other QSS solutions. An escape factor of zero has the radiative rates cancelling exactly, and thus tends more toward the Saha distribution. The local solution yields a population that is closer to the escape factor of unity, while the non-local calculation is closer to the zero escape factor. The radiance accumulated (Fig. 4(a)) follows the excited state populations, with the optically

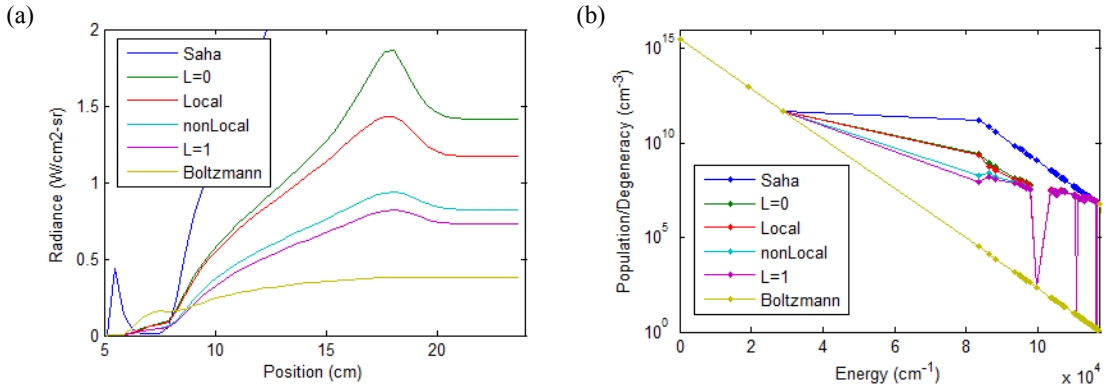

Fig. 4. Solutions obtained for different escape factor approximations. (a) Shows the accumulation of radiance over a backshell line of sight using different formulations for excited state calculations. The vehicle body is at ~25 cm while the shock edge is near 5 cm. (b) A Boltzmann plot of state populations for the N atom at ~17cm in (a).

thin case (Λ = 1) being the lowest of the four QSS simulations and the non-local solution being second, followed by the local and optically thick (Λ = 0) solutions. The heating estimate follows the trend in radiance, and is given in Table II. Approximately a 25% reduction in radiance is obtained by switching from the local to non-local solution method.

Table II. Heating solutions for a backshell case using different distributions and escape factor approximations in QSS.

Case	Q_{rad} (W/cm^2)
Boltzmann	2.08
Saha	291.36
$\Lambda = 0$	6.44
$\Lambda = 1$	3.62
Local	5.24
Non-local (tangent slab)	3.97
Non-local (weighted)	6.70

However, a limitation of the 1D non-local approach results from not accounting for radiance coming from the direction perpendicular to the line of sight. The tangent slab calculation evaluates the irradiance incident on a surface perpendicular to a line of sight. However, unlike surface heating, a gas volume element has no preferred orientation. Allowing for perpendicular radiation in the infinite slab geometry (i.e., by applying eq. (5) rather than the equations in Fig. 3), however, results in unrealistic spectral signatures in non-Boltzmann slabs and poor convergence as θ approaches $\pi/2$. An alternative approximation is to average the irradiance over a solid angle of 2π rather than 4π, which would correctly recover the Planck function in an optically thick equilibrium slab. This is denoted as "Non-local (weighted)" in Table II. This approach yielded a surface heating of 6.7 W/cm^2, which is actually larger than either the local or optically thick (Λ=0) solution. This approach unfortunately displays poor convergence properties, and as a result is not currently in the release version of NEQAIR. It is clear from this analysis that the method of approximating the non-local solution can dramatically alter the result. It appears likely that the full dimensional solution will differ significantly from the non-local solution based on 1D tangent slab. Further evaluation is necessary to resolve this issue.

5. TANGENT SLAB EVALUATION

The tangent slab calculation converts line radiance to an irradiance on a surface by performing an integral of radiance over the off-normal angle. The emission and absorption coefficients calculated from NEQAIR are re-used, meaning the 1D line-of-sight profile is taken to extend infinitely in all directions perpendicular to the line of sight. NEQAIR also has a spherical cap approximation which imposes curvature within the slabs by inserting geometric factors in the evaluation. The ensuing discussion also pertains to this mode of evaluation.

The difficulty in evaluating the tangent slab integral is that each angle requires a new line of sight evaluation, so is not computationally simple. Figure 4 shows three sample integrands that may be encountered in a tangent slab evaluation: depending on whether the slab is optically thin, thick or absorbing, a significantly different function may be encountered, so the optimum selection of integration points would not be known *a priori*. It is likely that curves resembling each of these will be encountered at different wavelengths within the same simulation. Tests using equispaced angular integrals showed that as many as 1000 intervals were required to converge the solution. Earlier versions of NEQAIR evaluated the lines of sight at 10 degree increments and assigned unequal weighting factors to each of them. The weighted integral was found to

match the converged tangent slab solution to within 2% for most cases tested. The method proposed by Johnston[9], which requires the equivalent of two line of sight evaluations, was found to be within 5% of the converged answer. For NEQAIR 14.0, a new approach was developed to compute the integral rigorously with an iterative adaptive quadrature scheme.

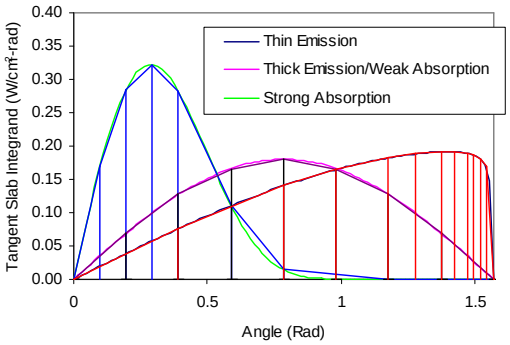

Fig. 5. Schematic of integration approach on three sample tangent slab integrands.

The scheme uses the bisection method with trapezoidal integration and involves successively dividing the region of integration until further division produces negligible refinement in the solution. Rather than dividing the entire range of the integral on each refinement, which would require 2^N line of sight evaluations, individual regions are bisected recursively, so that refinement is only performed where it is necessary to do so. This is shown schematically in Fig. 4, where the integration points are clustered so as to have the most impact on the error, as determined by the recursive evaluations. Furthermore, regions where the integrand is largest are converged first, so that less refinement is required in areas that contribute weakly to the overall integral. In practice, the most refined regions were found to be bisected up to 6 times, though the number of line of sight evaluations to obtain an answer within 1% of the full solution was typically between 8-13. In order to take advantage of array based operations without introducing unnecessary convergence steps, the wavelength grid points are sorted by optical depth and converged in blocks.

6. CO_2 RADIATION

The most recent version of the Carbon Dioxide Spectroscopic Databank, CDSD-4000,[10] is the most extensive line list for CO_2 presently available. CDSD-4000 is intended to be capable of simulating CO_2 spectra at temperatures up to 5000 K. The sheer number of lines and the size of the database make their inclusion in NEQAIR impractical, so a reduced form of the database has been incorporated by using a pseudo-continuum approach.[11] The NEQAIR CO_2 model contains 876,000 lines and covers all known CO_2 IR band systems, including the bands at 2.0, 2.7, and 4.3 μm. The approach to implementing this model involved retaining lines with relevance up to 8,000 K and parameterizing the remaining lines as a two-temperature dependent pseudo-continuum. The implementation and validation of this model is discussed in greater detail in Ref [11].

7. CFD/QSS INCONSISTENCIES

Runaway solutions have sometimes been produced by NEQAIR's QSS routines when the assumptions of the input data were inconsistent with NEQAIR's rate calculations. Generally, failures of the QSS equations to balance are encountered in cases of extreme non-equilibrium. Assuming the input dataset was generated by a CFD solver, such inconsistencies would suggest the CFD solution to be based on approximations that are inherently inconsistent with NEQAIR's underlying physics. This is usually observed when NEQAIR attempts to calculate forward and reverse rates for one of two sets of state specific reactions.

The first involves the balance of dissociation and recombination within molecular QSS:

$$AB(j) + M \rightleftarrows A + B + M \tag{8}$$

whereby an excited molecule may dissociate into its atomic constituents. The dissociation rate is hard-coded in NEQAIR in Arrhenius format, and is controlled by T_t for heavy particle collisions and sqrt(T_t-T_v) for electron collisions. A consistent QSS/CFD solution would have the summation of dissociation rates by level equal to the overall reaction rate. However, this is not generally enforceable, nor is it strictly necessary. Problems may arise, however, in the calculation of the reverse rate. NEQAIR uses partition functions to calculate the equilibrium coefficient. That is:

$$K_{eq} = \frac{k_r}{k_f} = \frac{Q_A Q_B}{Q_{AB}} e^{-\Delta E_{rxn}/kT} \tag{9}$$

In NEQAIR's four-temperature model, the partition functions would logically be calculated assuming separation of modes applies, i.e.:

$$Q_{AB} = Q_t(T_t) \sum_{n=1}^{n_{\max}} g_n \exp\left(-\frac{E_n}{kT_e}\right) \sum_{\upsilon=0}^{\upsilon_{\max}(n)} \exp\left(-\frac{E_\upsilon}{kT_\upsilon}\right) \sum_{J=0}^{J_{\max}(\upsilon,n)} (2J+1) \exp\left(-\frac{E_J}{kT_r}\right) \tag{10}$$

In this way, a reverse rate coefficient is obtained that follows microscopic reversibility principles under a four-temperature model. However, the reverse rate

obtained this way has a complicated dependence on temperature which is generally inconsistent with standard CFD calculations. The result was that NEQAIR's reverse rate coefficient could predict recombination rates which were orders of magnitude faster than those used in CFD. This would produce a very large concentration of excited molecular states which then leads to excessive molecular radiation. In the extreme, the molecular state balance could fail to close, leading to unpredictable results. This was partially mitigated in older versions of NEQAIR by switching QSS off for low electron mole fraction. The problem with this approach is that it would sometimes disable QSS when it was not necessary or desirable to do so.

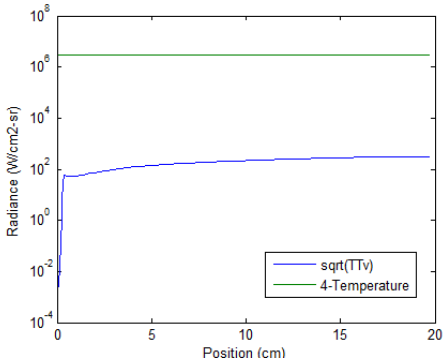

Fig. 6. Accumulated radiance versus position for a high speed air entry case. Plots show results using different controlling temperatures for radiative recombination.

The mitigation introduced in NEQAIR 14.0 was to calculate the partition function according to the same temperatures used for the forward reactions, that is sqrt(T_tT_v) for electron impact and T_t for heavy particles. The reverse of spontaneous dissociation, which was added in v14.0, still uses the four-temperature partition function. While using effective temperatures is undesirable from the standpoint of adhering to principles of detailed balance, it was considered necessary for code usability. Also, it recovers the correct and identical results when the four temperatures collapse to a single temperature. Fig. 6 shows an example solution when different rate controlling reactions are used, with the radiance plotted as the accumulated radiance over the line of sight. With the 4-temperature equilibrium constant, the solution blows up early in the line of sight and never recovers to a reasonable value. In this case, the additional radiance is caused by N^+ and N recombination to an emitting state of N_2^+. Using the different controlling reactions eliminates the issue without requiring limiters on the QSS solution range.

The second difficulty observed occurs in the ionization reactions of the atom mole balance:

$$A(j)+M \rightleftarrows A^+ + e^- + M$$

The forward rate coefficients for impact dissociation are hard-coded into NEQAIR. Reverse rate coefficients are computed from Saha equilibrium based on the *electronic* temperature (T_e). This is consistent with CFD practices. However, NEQAIR does not carry a separate *electron* temperature (T_{el}), rather it is assumed that the electron and electronic temperature are the same. Similarly, most CFD codes do not carry a separate electron or electronic temperature and the electron temperature is set equal to either T_t or T_v. For radiation calculations, it is known that the most realistic results are obtained when $T_e = T_v$. Therefore, this is typically done when transferring a CFD solution to NEQAIR. A difficulty can arise when a CFD result obtained with $T_{el} = T_t$ is transcribed to NEQAIR while setting $T_e = T_v$. The reason for this is shown schematically in the Boltzmann diagram of Fig. 7. The CFD calculation may yield an ion density near the Saha equilibrium driven by T_t, which is orders of magnitude higher than what would be given by T_v. If NEQAIR then uses this point with T_v to derive an excited state density, the result may be far in excess of that derived by either temperature alone, and may even exceed the ground state density.

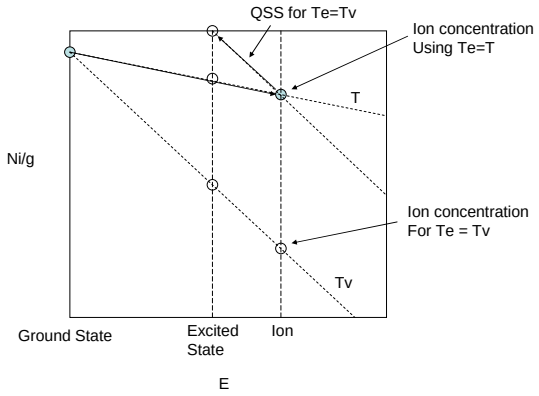

Fig. 7. Boltzmann Diagram showing how inconsistent T/T_v treatment can result in unrealistic state populations.

NEQAIR 14 may write warnings when this is likely to occur, but does not halt execution as there are some physically realistic cases which display similar characteristics. An example where this occurs is given in Fig. 8. In this case, the Boltzmann solution is lower than the QSS solution in the non-equilibrium region. This is contrary to usual predictions and also inconsistent with shock tube data in this regime,[12] which is more consistent with the Boltzmann result. Running QSS with T_e set equal to T_t creates an overly excited population, resulting in a larger radiance accumulated along the line of sight. While setting $T_e = T_v$ gives a lower overall radiative flux, the non-equilibrium overshoot is more pronounced for reasons

discussed above. In terms of the wall-directed heat flux, the QSS result is 44 and 13% greater than the Boltzmann solution for these cases, respectively.

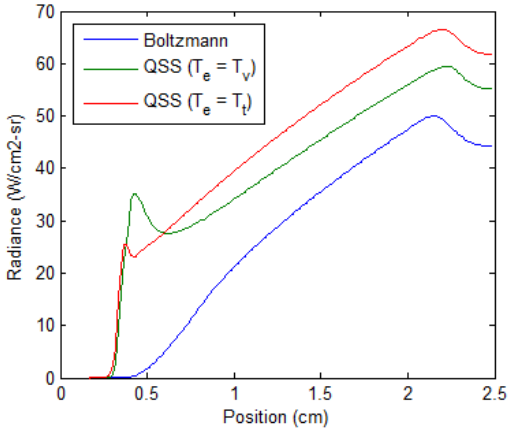

Fig. 8. Radiance accumulated on the line of sight for high speed air entry using different QSS options when the CFD solution uses $T_e = T_t$.

8. CONCLUSIONS

This paper has discussed various aspects of the recent updates to the NEQAIR code. Parallelization of the radiation computation has reduced the evaluation time by around 30× when sufficient processors are available. A new implementation for continuum radiation based on TOPBase has improved predictions in the ultraviolet and at high ionization when compared to shock tube data. The implementation of a non-local transport solver allows for better radiation predictions in backshell cases and highly absorbing boundary layers. The inclusion of infrared CO_2 radiation based on CDSD-4000 allows for prediction of radiative heating at low velocity Martian conditions. An adaptive tangent slab routine is presented which converges the radiation transport solution to within 1% with minimal performance penalty. Finally, a discussion of QSS/CFD inconsistencies which lead to erroneous and/or unbounded results has been presented.

Some desired areas for improvement and future development for NEQAIR are suggested. In particular, the non-local solution is found to be sensitive to how the dimensionality of the problem is approximated, and this requires further examination. Additionally, molecular non-local calculations remain to be implemented. The QSS/CFD inconsistencies point to a need to improve the manner of integrating radiation and fluid dynamics codes. Finally, inclusion of ablation products and 3D integration are still required to complete the full potential of NEQAIR.

9. REFERENCES

1. Park, C., "Nonequilibrium Air Radiation (NEQAIR) Program: User's Manual," NASA TM 86707.
2. Whiting, E., Park, C., Liu, Y., Arnold, J., and Paterson, J., "NEQAIR96, Nonequilibrium and Equilibrium Radiative Transport and Spectra Program: User's Manual," NASA RP-1389, 1996.
3. Peach, G., "Continuous absorption coefficients for non-hydrogenic atoms," *Memoirs of the Royal Astronomical Society,* Vol. 73, 1970, pp. 1-123.
4. Cunto, W., Mendoza, C., Ochsenbein, F., and Zeippen, C., "TOPbase at the CDS," *The Opacity Project: Selected research papers-Atomic Data Tables for S to Fe,* Vol. 2, 1994, p. 53.
5. Bose, D., McCorkle, E., Bogdanoff, D., and Gary A. Allen, J., "Comparisons of Air Radiation Model with Shock Tube Measurements," AIAA 2009-1030.
6. Brandis, A. M., Cruden, B. A., Prabhu, D., Johnston, C. O., and Bose, D., "Uncertainty Analysis of NEQAIR and HARA Predictions of Air Radiation Measurements Obtained in the EAST Facility," AIAA Paper 2011-3478, June 2011.
7. Cruden, B. A., Prabhu, D., and Martinez, R., "Absolute Radiation Measurement in Venus and Mars Entry Conditions," *Journal of Spacecraft and Rockets,* Vol. 49, No. 6, 2012, pp. 1069-1079.
8. Johnston, C., Brandis, A., Panesi, M., and Sutton, K., "Shock Layer Radiation Modeling and Uncertainty for Mars Entry," *43rd AIAA Thermophysics Conference*. New Orleans, Louisiana, 2012, AIAA-2012-2866.
9. Johnston, C. O., "Improved Exponential Integral Approximation for Tangent-Slab Radiation Transport," *Journal of Thermophysics and Heat Transfer,* Vol. 24, No. 3, 2010, pp. 659-661.
10. Tashkun, S. A., and Perevalov, V. I., "CDSD-4000: High-resolution, high-temperature carbon dioxide spectroscopic databank," *Journal of Quantitative Spectroscopy and Radiative Transfer,* Vol. 112, 2011, pp. 1403-1410.
11. Palmer, G., and Cruden, B., "Experimental Validation of CO_2 Radiation Simulations," AIAA Paper 2012-3188.
12. Brandis, A., Johnston, C., Cruden, B., Prabhu, D., and Bose, D., "Validation of High Speed Earth Atmospheric Entry Radiative Heating from 9.5 to 15.5 km/s," *43rd AIAA Thermophysics Conference*. AIAA, New Orleans, Louisiana, 2012, AIAA-2012-2865.